JOINT EUROPEAN TORUS

JET–P(93)44

A.V. Chankin, D.D.R. Summers, H.J. Jäckel,
M. LeSourd, G.F. Matthews, R. Reichle

Infra-Red Measurements of the Divertor Power at JET

Infra-Red Measurements of the Divertor Power at JET

A.V. Chankin[1], D.D.R. Summers, H.J. Jäckel,
M. LeSourd, G.F. Matthews, R. Reichle

JET-Joint Undertaking, Culham Science Centre, OX14 3DB, Abingdon, UK

[1]I.V. Kurchatov Institute for Fusion Research, Moscow, Russia.

Preprint of a paper to be submitted for publication in
Plasma Physics and Contolled Fusion.
June 1993

ABSTRACT

An infrared camera has been used to check the power balance calculations in a series of JET divertor discharges. The discharges spanned the density range $\langle n_e \rangle = 1 - 7 \times 10^{19} m^{-3}$, with the highest densities achieved by neutral beam heating and intensive gas puffing.

For the discharges in which IR data were taken, the total power to the target, as deduced from the IR signal, was proportional to the expected divertor target power estimated from $P_{in}-P_{rad}-\dot{W}$, where P_{in} is the input power to the plasma, P_{rad} - measured radiated power and $\dot{W}$ is the rate of change in the plasma stored energy. Close proportionality, pointing to good power balance, has been achieved in Ohmic plasmas, as well as in L- and H-modes with either RF and/or NB heating up to 22MW, of which up to 12MW was monitored on the target as heat deposition by the IR system. Analysis of the data has shown no systematic trends of deteriorating power balance with increasing volume averaged density or with heating power.

1. INTRODUCTION

It is often observed that the power to the target of divertor tokamaks calculated from Langmuir probe and infrared data, is less than that evaluated from energy balance considerations. The difference is more pronounced in the H-modes (see e.g. The JET Team, 1992, Leonard et al., 1992, ASDEX Team, 1989). The expected power load of the divertor target tiles P_{target} is calculated from $P_{in}-P_{rad}-\dot{W}$, where P_{in} is the input power to the plasma, P_{rad} includes all sources of radiation and neutral particles. $\dot{W} = dW/dt$ is the rate of change in plasma stored energy. In certain discharge conditions like a "radiative divertor", where most of the power crossing the magnetic separatrix does not reach the target because of strong radiation at the edge, different terms in $P_{in}-P_{rad}-\dot{W}$ almost cancel each other, and the remaining flux, P_{target}, is small. In such conditions, uncertainties in measuring P_{in}, $\dot{W}$ and P_{rad} do not allow to check the consistency between the experimentally measured power to the target, P_{exp}, and $P_{in}-P_{rad}-\dot{W}$. Therefore, the real problem of deficit in the power balance only arises when the expected P_{target} is comparable to P_{in}.

The problem of hidden power loss channels was first pointed out by the ASDEX Team (1989), where reduced power flux to the divertor, observed immediately

after the L-H transition and measured with Langmuir probes and infrared cameras, did not recover and remained at a low level long after the transition, when the new steady state conditions of an H-mode had been established. A number of possible reasons have been suggested to explain the power deficit. They are: additional charge exchange losses whereby power is deposited onto the walls around the main plasma: asymmetries or toroidal variations of the power deposited in the divertor channel; losses by fast ions in orbits that can deviate strongly from the magnetic separatrix and create a power deposition region outside the field of view of the IR camera.

During an ELMy H-mode in DIII-D (Leonard et al., 1992) the power load to the divertor target, measured with the IR camera, was 2 - 8 times smaller than expected, leading to inability to account for 25 - 50% of the input power. Examination of possible hidden loss mechanisms, including toroidal asymmetries in power deposition and charge exchange losses, has so far failed to explain fully the missing power.

At JET (The JET Team, 1992) the power deposited on the target was evaluated from probe measurements, assuming equality of ion and electron temperatures and using the observed profiles of N_e and T_e. The discharges analysed were in the single null configuration with NB power from 2 to 10MW. The Langmuir probes showed a fairly good power balance in the L-mode phase of these discharges, but with increasing NBI power that caused transition to an H-mode, only a fraction of the power to the target calculated from the global power balance, was detected by the probes. The discrepancy increased at high densities, when probe measured powers were often only 25 to 40% of the expected. Calculation of CX losses arising from the recycling neutrals produced a figure for possible power loss of the order of 1 to 2MW, although the discrepancy in power was about 3MW at high densities. At JET a large fraction of this power loss by CX probably could not be observed by the JET bolometer system. The correction made for these undetected losses has helped to reduce the discrepancy, but does not eliminate it completely.

At DIII-D (Leonard et al., 1992) CX losses as a possible candidate to explain poor power balance in the H-modes have been ruled out, as it was found that, in the regimes or radiating divertor and high neutral pressures, total losses did not increase significantly when the neutral pressure at the midplane was changed by a factor of 6. The inability to account for the missing power due to undetected CX losses at DIII-D has also been confirmed by DEGAS code modelling.

Another possible explanation for the missing power at JET could be a large ratio of ion to electron temperature at the target, while it was assumed that $T_i = T_e$ in calculation of the conducted power from the Langmuir probe data. However, edge code simulations have shown that equipartition between electrons and ions should produce electron temperatures significantly higher than those measured.

Summarising the present situation with power balance calculations, we can say that a limited number of observations from large machines point to the problem of identification of loss channels of power conducted to the scrape-off layer (SOL) plasma, especially in the H-mode. Available experimental information is incomplete and inadequate even to single out one or two possible mechanisms (or unmeasured loss sources), responsible for a deterioration of power balance. The problem is of great importance, as proper identification of power loss mechanisms is needed to verify and benchmark SOL and divertor models and predictive codes.

In this paper we present some experimental data from JET that have become available after the installation of an IR camera in the 1991-92 experimental campaign. Geometrical limitations and the complicated target tile structure at JET limited the number of discharges successfully recorded by the IR camera and restricted the applicability of the diagnostics in obtaining the heat deposition profiles from the 2D temperature distribution. However, the IR camera could serve well as a monitor of total power deposited onto the target in some of the regimes, enabling us to check the power balance in JET with different densities and input powers in X-point discharges. It was found that deposited power measured with the IR detector matched very well the expected divertor target power $P_{in}-P_{rad}-\dot{W}$ during Ohmic heating, L-and H-modes.

2. EXPERIMENTAL SET UP

The infrared camera was mounted on a horizontal port, viewing the top target tiles which were made of Carbon Fibre Composite, as shown on Fig. 1. Beryllium was used as the material for the bottom tiles. The detector of the IR camera was a focal plane array, consisted of 32 × 32 CdHgT diodes, maintained at – 80°C by a Peltier cooler. The detector was preset to measure surface temperatures in the range 300 - 1600°C. A filter was used to restrict the waveband to 3 - 5μm in order to avoid spectral lines. A single lens optical system focused a target area

~ 32 × 25cm^2 onto the detector surface, providing ~ 0.8 - 1.0cm spatial resolution. The associated data acquisition system allowed the array to be sampled at intervals throughout plasma pulses. Thus, an almost continuous thermal picture of the target could be obtained, from which a time-resolved evaluation could be made of the power flux. Typical time resolution was 80ms.

In order to shadow any sharp edges caused by misalignment of the tiles relative to the plasma flux surfaces, the four bands of Carbon tiles on the high field side of the target were sloped towards their edges (see e.g. Pick et al., 1992). Fig. 2 gives the picture of the part of the top target with the area covered by the IR camera mapped onto it.

Fig. 3 shows a close-up photograph taken of the part of the target, viewed by the camera. Some surface features are marked for comparison with a typical 2D power distribution, presented in Fig. 4. As is clear from Figs 3 and 4, the heat deposition pattern is very non-uniform, with power flux concentrated on the exposed edges. After the temperature of the hot spots in the series of the discharges analysed reached 1600°C, extrapolation from neighbouring pixels was used to estimate the power density at the hottest zones. However, power flow to the areas with temperatures above 1600°C was very small compared to the total power flow.

A simple semi-infinite one-dimensional model for heat deposition (Carslaw and Jaeger, 1959) was used to obtain the power distribution from temperature distribution, assuming that the power flux was constant between the two successive measurement times. So, the effect of single step of power density, p, of the duration t_p on surface temperature was calculated as:

$$T - T_0 = Kp\sqrt{t}, \quad \text{for } t \le t_p,$$
$$T - T_0 = Kp\left(\sqrt{t} - \sqrt{t - t_p}\right), \quad \text{for } t > t_p,$$

with $K = \sqrt{2/\pi\rho kc}$,where ρ is density, k - thermal conductivity, c - the specific heat. We used constant coefficient K = 0.91cm^{2}W^{-1}sec$^{-0.5}$, as it was previously done by Reichle et al. (1990). The spectral emissivity of the Carbon surface in the 3 - 5μm was assumed to be 90%.

The effect of poor spatial resolution of the detector in the presence of highly distinguishable hot spots was partly compensated by the quasi-linear response of the detector signal to the surface temperature.

For all of the discharges analysed the direction of ion grad-B drift was towards the upper target, and the direction of plasma current was clockwise, if viewed from the top. In such a configuration, plasma particles, approaching the target surface along the magnetic field lines, moved from the right to the left at the inner strike zone and in the opposite direction at the outer strike zone, as shown in Fig. 3 by the arrows. Taking into account the exact surface structure and small angles (~ 1^{o}) between the magnetic field lines and the surface, it appeared that a large part of the surface at the outer strike zone (upper right corner on Fig. 3) should have been shadowed, while the inner strike zone should have received the full power exposure, as if it was a flat tile area. This raises the question as to whether the part of the target surface viewed by the IR camera was representative of the whole surface.

The total power flux to the top target was calculated by multiplying the integrated power deposition, registered by the camera, by a geometrical factor, reflecting the fraction of the whole toroidal transit ($2\pi R$), viewed by the IR camera. In order to correct the effect of shadowing of the target at the outer strike zone, a weighting factor was used for the power onto the outer side, reflecting the geometrical extent of the shadowing. This factor was a time independent function of major radius. The same procedure has been used to correct the poloidal profiles of the deposited power. These profiles were generated by averaging the powers along the toroidal lines. An example of the poloidal profile for the same shot, as shown in Fig. 4, is presented in Fig. 5A. The corrected profile, accounting for the shadowing on the outer strike zone, is shown in Fig. 5b. The correction has obviously increased calculated power to the outer strike zone. Overall, comparing total calculated powers to the target, P_{exp}, with $P_{in}-P_{rad}-\dot{W}$, it was found that the correction has improved the correspondence between P_{exp} and $P_{in}-P_{rad}-\dot{W}$.

Because of the complexity and inhomogeneity of the target surface, producing a series of hot spots on camera images, poloidal profiles were considered not to be reliable on their own. The peculiarities of the target surface could have distorted poloidal profiles. An example of such a distortion is manifested by a rise in power density seen at small major radii, $R \approx 232$cm, in Fig. 5a, b. That has apparently been produced by a hot spot seen in the lower right hand corner in Fig. 4.

3. RESULTS AND DISCUSSIONS

The discharges analysed were Double Null X-point discharges, but with predominant interaction on the top Carbon target. Interactions with other surfaces including the bottom target tiles, inner wall and RF antennas, have been monitored by a number of bolometer chords and wide-angled CCD cameras. The X-point to target distance was varied from –2 (X-point outside plasma) to + 4cm (X-point inside plasma). The discharges spanned the density range $\langle n_e \rangle = 1 - 7 \times 10^{19} m^{-3}$ with the highest densities achieved by neutral beam heating and strong gas puffing. Maximum total power input to the plasma reached 22MW.

Contrary to what has been concluded earlier at JET from target power flux measurements with Langmuir probes (The JET Team, 1992), the data obtained with the IR camera allow one to conclude that the power balance is kept very well. Throughout the series of shots where infrared measurements were taken, a fairly good power balance has been obtained in Ohmic heating, L- and H-modes. The correction introduced to account for the partial shadowing of the tiles located on the outer strike zone, as explained in the previous section, was found to improve the consistency between P_{exp} $P_{in}-P_{rad}-\dot{W}$.

A typical example of the comparison between P_{exp} and $P_{in}-P_{rad}-\dot{W}$ for a discharge with high input power is given in Fig. 6. Up to 22MW of additional power (13MW of NB and 9MW of RF power) was deposited into the plasma. The top X-point to target distance was kept within 0 - 3cm (X-point outside plasma) between 7s and 9.7s, and no interaction with other surfaces was detected. The discharge has undergone an L-H transition at 7.45s and the sudden disappearance of the ELM activity at 8.12s, shortly after the NB power was turned on. The transition from the H-mode back to the L-mode at 9.03s was caused by the reduction in the heating power. As can be seen from the upper plot in Fig. 6, the power balance is kept well in both L- and H-phases. The maximum power flow to the target, calculated from the IR measurements, reached 11MW at ≈ 8.8s. At that time about 9MW were radiated (P_{rad}, measured by the bolometer system), and the rest of the power accounts for the rate of change in energy content, $\dot{W}$. The lack of power balance, evident at ≈ 9.3 and ≈ 9.7s (after the heating power was stepped down), can be partially explained by fluctuations in $P_{in}-P_{rad}-\dot{W}$, caused by fluctuations in W measurements. Between 9.1 and 9.6s, the top X-point to target

distance was near zero, and no evidence of interaction with other surfaces, apart from the top target, was detected. The volume averaged density in this discharge reached $6 \times 10^{19}m^{-3}$ just before the H-L transition and was achieved, in addition to the contribution from the NB particle input ($1 \times 10^{21}s^{-1}$), by strong gas puffing at $6 \times 10^{21}s^{-1}$. Fig. 7 represents an X-point discharge (top X-point is formed between 4.7 and 8.2s and X-point to target distance is 4cm between 6 and 8s with X-point located inside plasma) with a sharp L-H transition. The transition occurred at 6.14s. The volume averaged density reached $\approx 5 \times 10^{19}m^{-3}$ by the end of the H-mode phase. The gas puffing was sharply reduced between 6.5 and 8.0s. Again, as can be seen from the upper plot in Fig. 7, the power balance is kept well in both the L-and H-phases of the discharge. There was evidence of some plasma interaction with the bottom target in this discharge, gradually disappearing during the H-mode. However, that interaction (if strong enough) could only reduce the power, measured by the infrared system on the top target. As no significant power deficit (hidden power losses) was recorded, we may assume that power flow to the bottom target was small. The time evolution of the poloidal profile of power flux for this discharge is shown in Fig. 5b.

An example of a discharge with an extended H-mode phase is shown in Fig. 8. The toroidal field was only 1.65T in this discharge, and the L-H transition occurred at low NB power, 2MW. Throughout this discharge a number of giant sawteeth caused jumps in P_{exp}. No gas puffing was applied between 5 and 8s, and the top X-point was 2cm inside plasma. No evidence of plasma interaction with other surfaces was detected in this discharge.

Statistical analysis of the correspondence between P_{exp} and $P_{in}-P_{rad}-\dot{W}$ has been performed by Jäckel et al. (1993). The discharges selected were ones in which, according to a magnetic equilibrium, most of the power must have been deposited onto the top target. This analysis has shown that the data available do not indicate any systematic difference in power accountability between the L- and H-modes. That is in apparent disagreement with the poor power balance in the H-modes reported earlier. Likewise, no systematic trend of deterioration of power accountability has been observed with increasing plasma density.

However, two remarks should be made on what is defined here as a good power balance. As we have said in section 1, experimental uncertainties, mainly in measuring W and P_{rad}, do not allow us to make any conclusion on power balance when the expected power flow to the target, $P_{in}-P_{rad}-\dot{W}$, is too low.

Therefore, we only claim that in the conditions when the ratio $(P_{in}-P_{rad}-\dot{W})/P_{in}$ is not small, as was the case in the series of the discharges covered by the infrared measurements, no large fraction of power was missed. In absolute terms, uncertainties in $P_{in}-P_{rad}-\dot{W}$, which are of the order of 3MW, do not allow us to make power balance calculations with an accuracy better than that. Therefore, the effect on the power accountability of such mechanisms as charge exchange losses with power carried by neutrals to the walls, could not be properly assessed. Estimations of such losses have shown that they are of the order of 1 - 2MW at high densities (The JET Team, 1992), well within the experimental uncertainties of our measurements.

More detailed analysis of the data that we present here was hampered by damage to the Langmuir probes closest to the strike points, were the maxima of IR power have been observed.

One of the possible ways to reconcile experimental data on good power accountability, presented in this paper, with the poor power balance, obtained by the ASDEX Team (1989) and Leonard et al. (1992), would be to mention that present data from JET have been obtained with very small separations between the X-point and the target, contrary to ASDEX and DIII-D data. Although, we have no explanation for a mechanism that would result in such a dependence of the power balance on the separation of the X-point from the target.

4. ACKNOWLEDGEMENTS

The authors would like to acknowledge fruitful discussions with L. de Kock, P.J. Harbour and G.C. Vlases, and to thank K.M. Slavin and E. Oord for their help with the computer support.

References

[1] ASDEX Team (1989), The H-mode of ASDEX, Nucl. Fusion **29,** No. 11, 1959.

[2] Carslaw, M.S. and Jaeger, J.C. (1959), Conduction of Heat in Solids (Clarendon Press, Oxford).

[3] The JET Team (1992), (presented by G.C. Vlases), Divertor Physics at JET: Experimental Results and Modelling. Proc. of 14th Conf. on Plasma Physics and Controlled Nuclear Fusion Research, Würzburg, Germany.

[4] Jäckel, H.J. et al. (1993), to be published in Proc. of 20th European Conf. on Contr. Fusion and Plasma Physics.

[5] Leonard, A.W. et al. (1992), Power Balance and Divertor Performance in DIII-D, APS paper No. 8Q 1, Seattle, USA.

[6] Pick, M.A. et al (1992), J. Nucl. Mater. 196-198, **215**.

[7] Reichle, R., Summers, D.D.R. and Stamp, M.F., J. Nucl. Mater. 176 & 177, **375**.

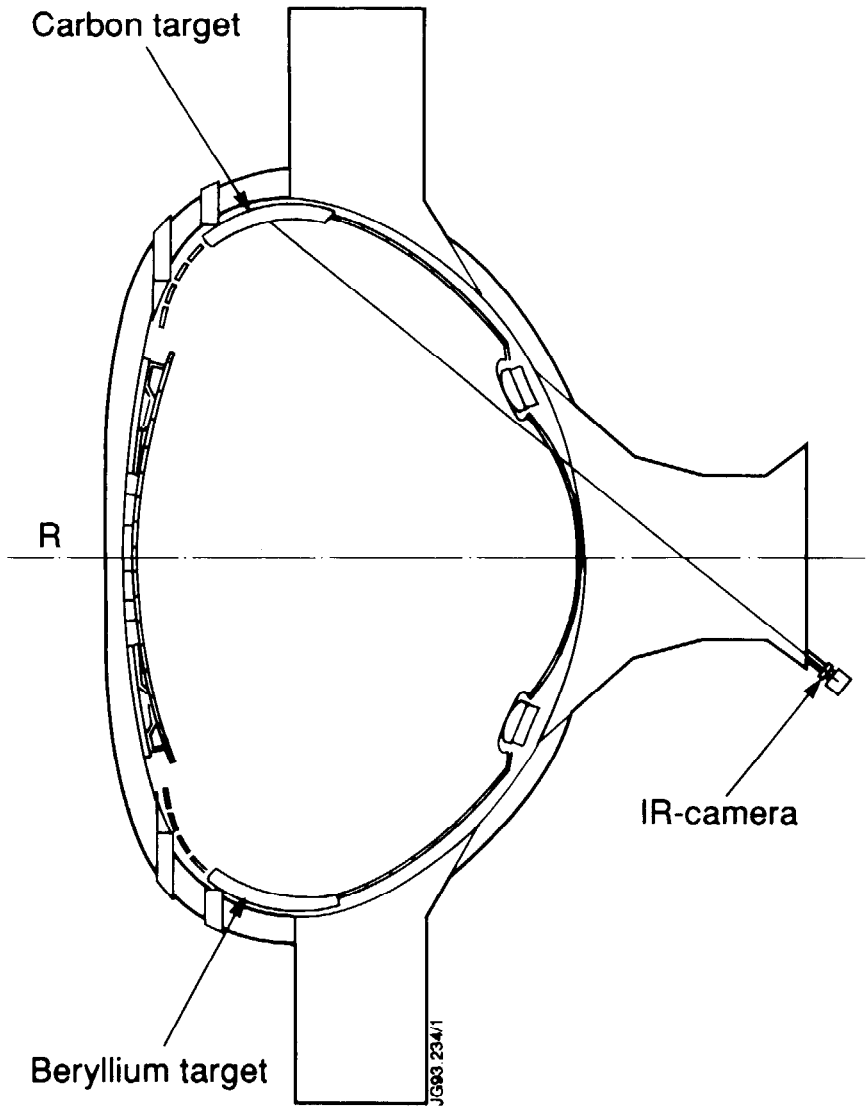

Fig. 1 Poloidal cross-section of the JET vessel, showing the position of the IR camera.

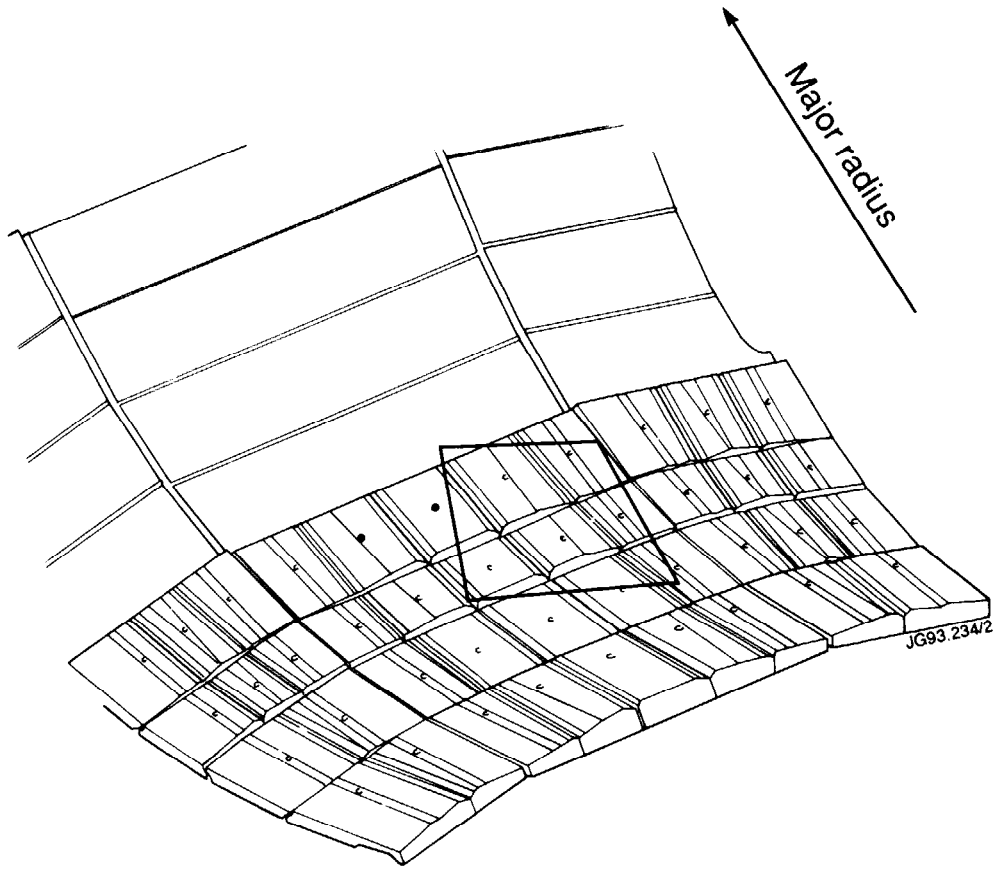

Fig. 2 Part of the top target with the area covered by the IR camera indicated on it.

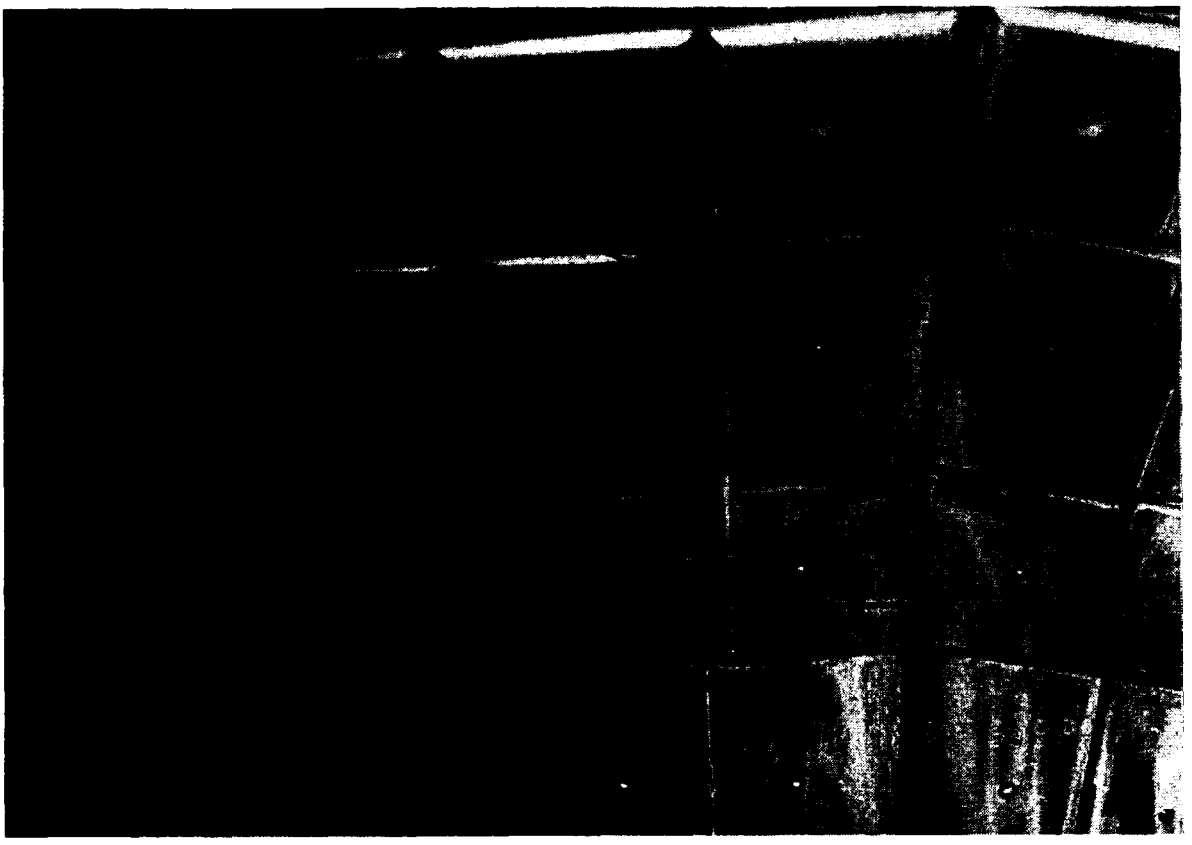

Fig. 3. Close-up photograph of the part of the target viewed by the IR camera.

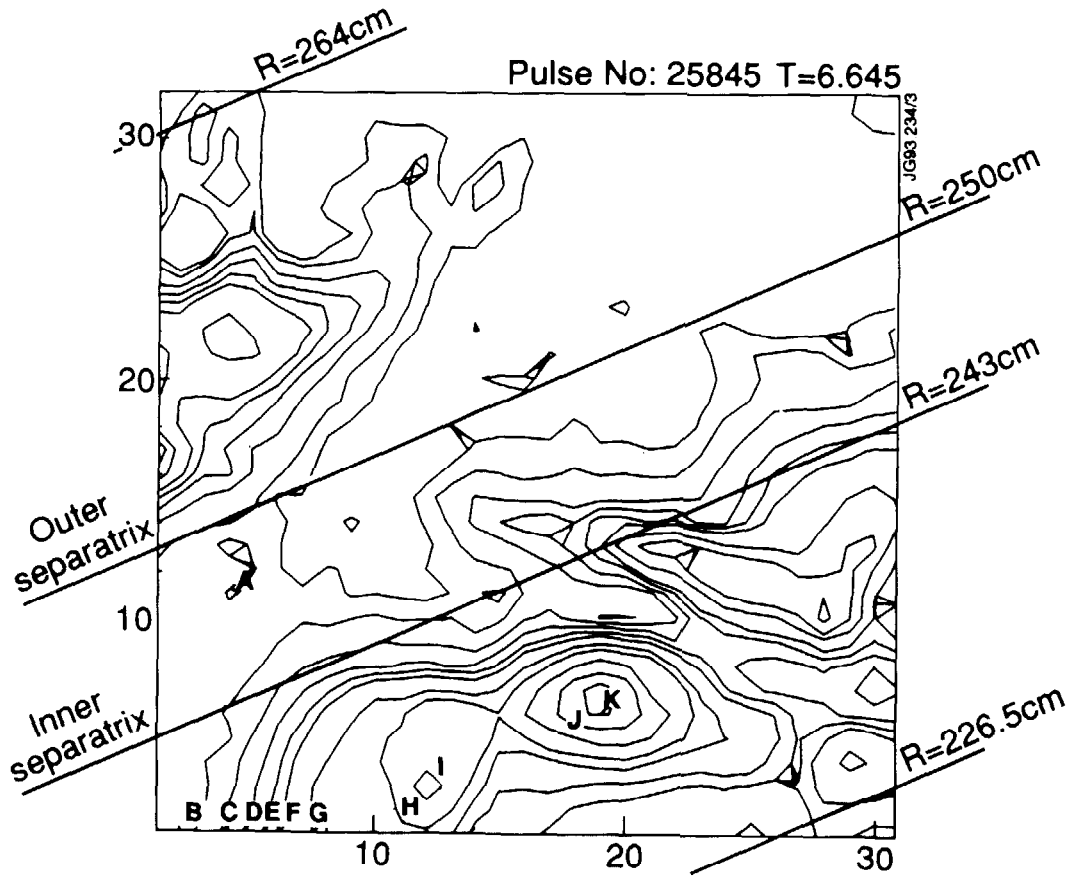

Fig. 4 Iso-contour plot of power density onto the target, obtained by the IR camera. Contour levels (in W/cm^2) correspond to: A–10, B–20, C–40, D–60, E–80, F–100, G–150, H–200, J–450, K–600.

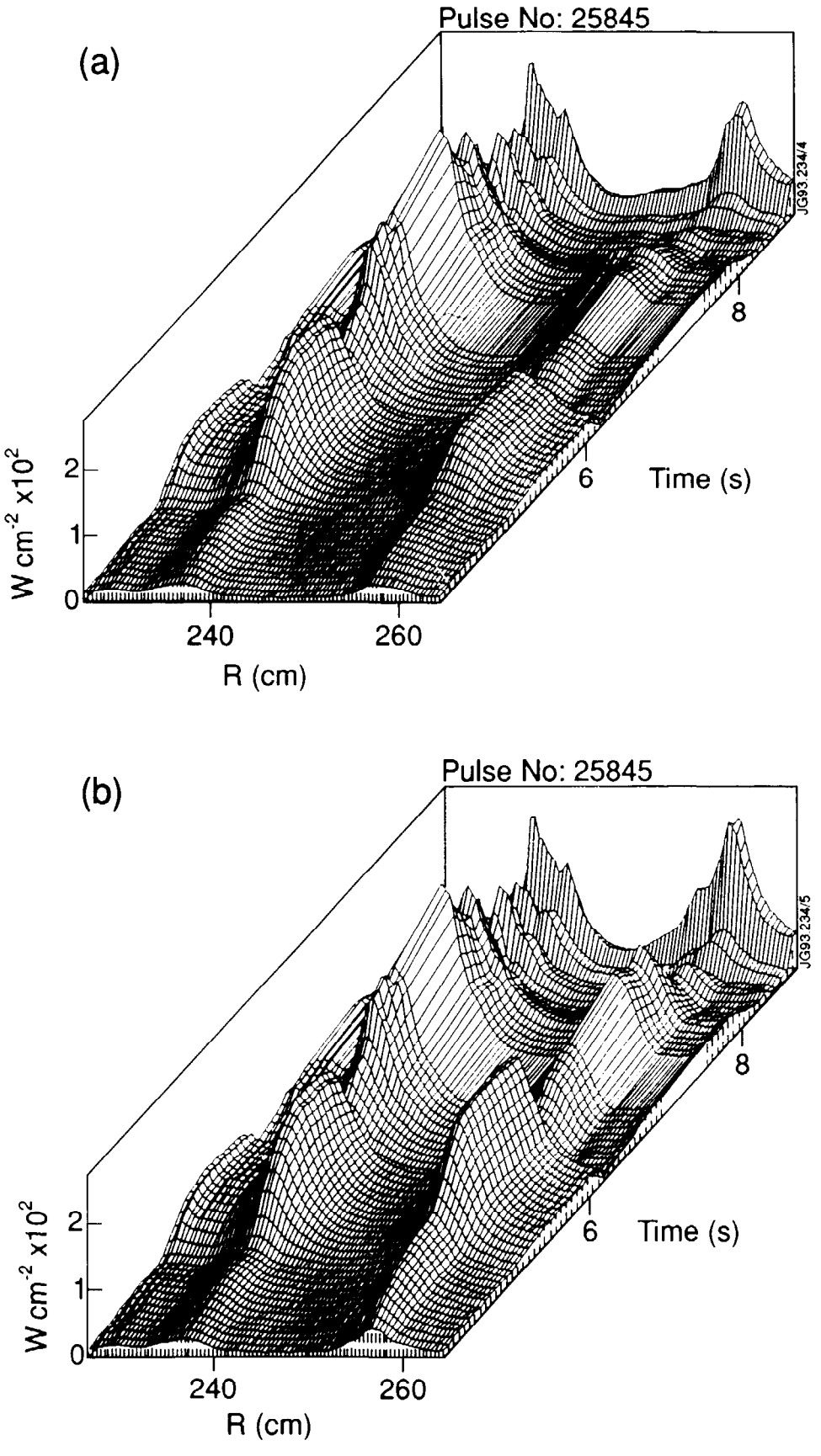

Fig. 5 Time evolution of the poloidal profiles of deposited power, without (a) and with (b) the correction made to account for the shadowing on the outer strike zone.

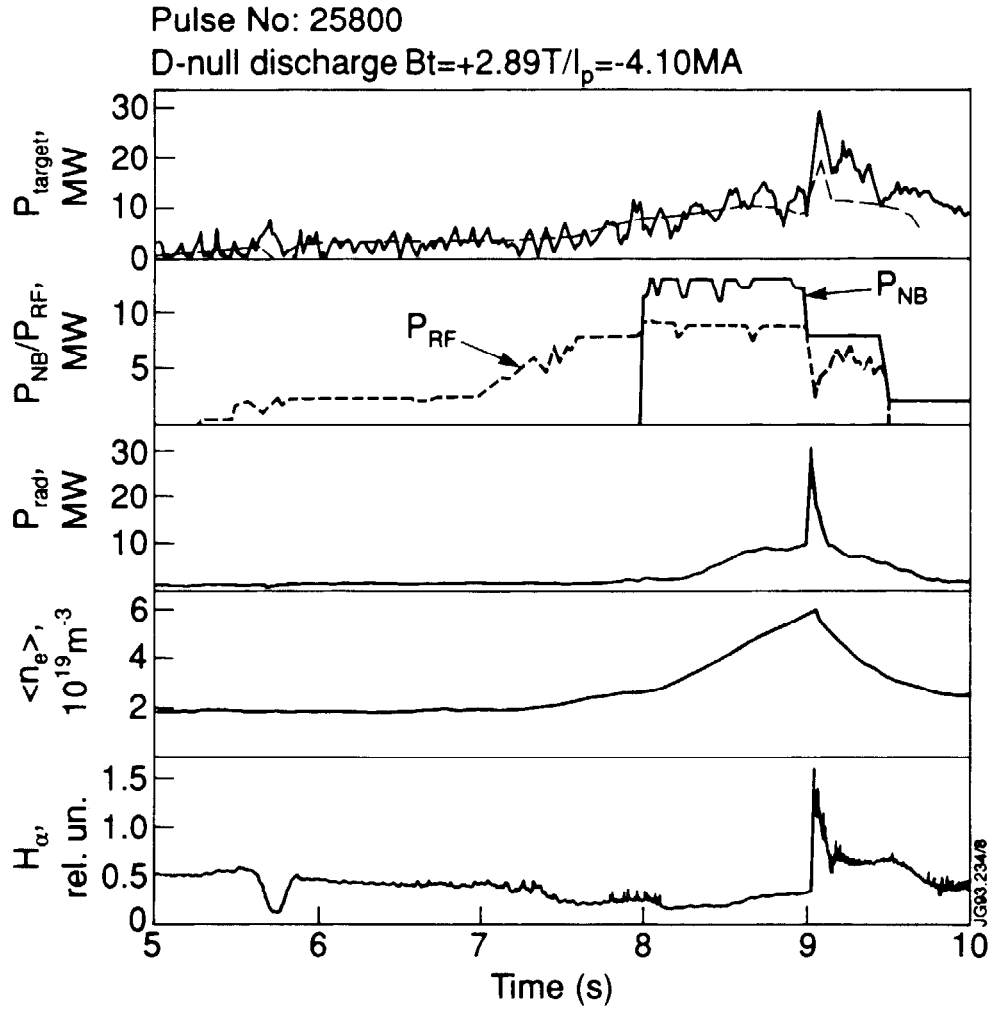

Fig. 6 Comparison between P_{exp} (solid line on the top plot) and $P_{in}-P_{rad}-\dot{W}$ (dashed-dotted line). Other parameters shown are: input NB and RF powers, radiated power, P_{rad}, volume averaged density, $\langle n_e \rangle$, and H_α spectral line intensity from a vertical line looking at the divertor.

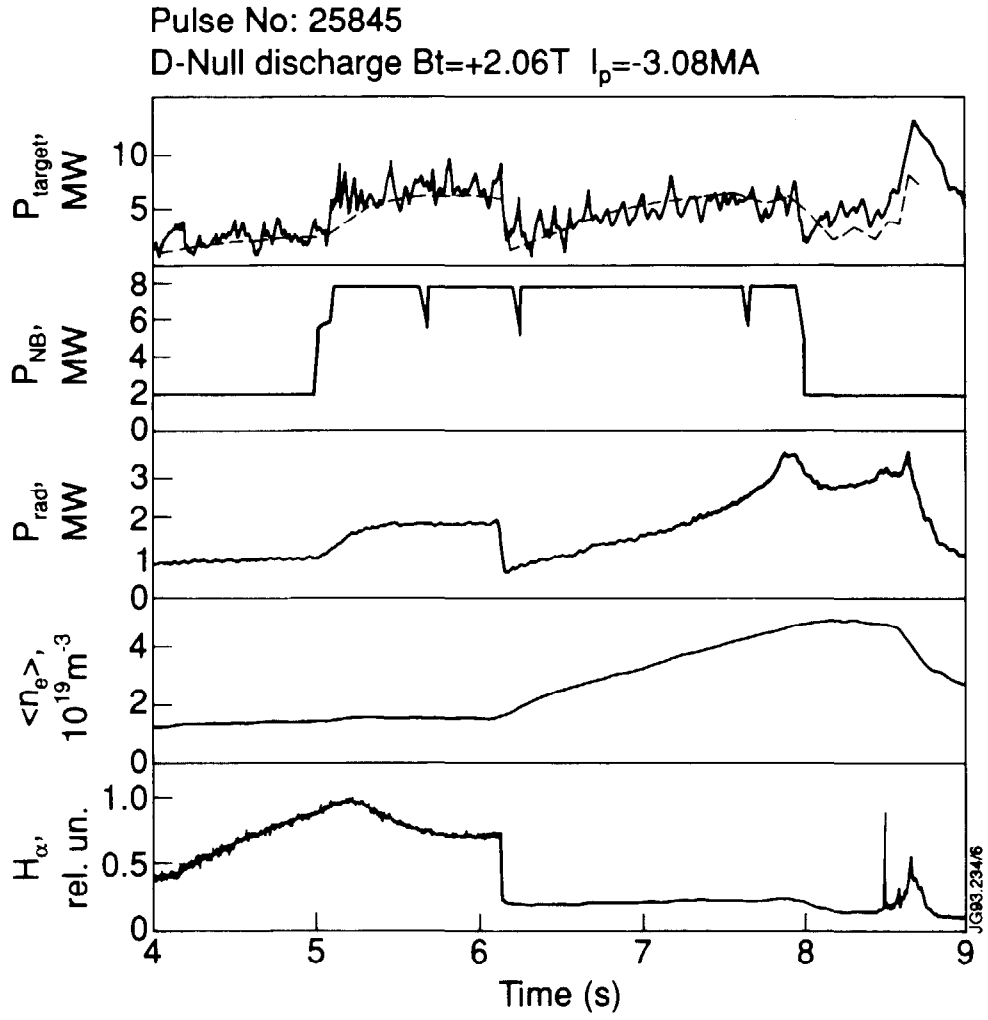

Fig. 7 Comparison between P_{exp} (solid line on the top plot) and $P_{in}-P_{rad}-\dot{W}$ (dashed-dotted line). Designations are the same as in Fig. 6.

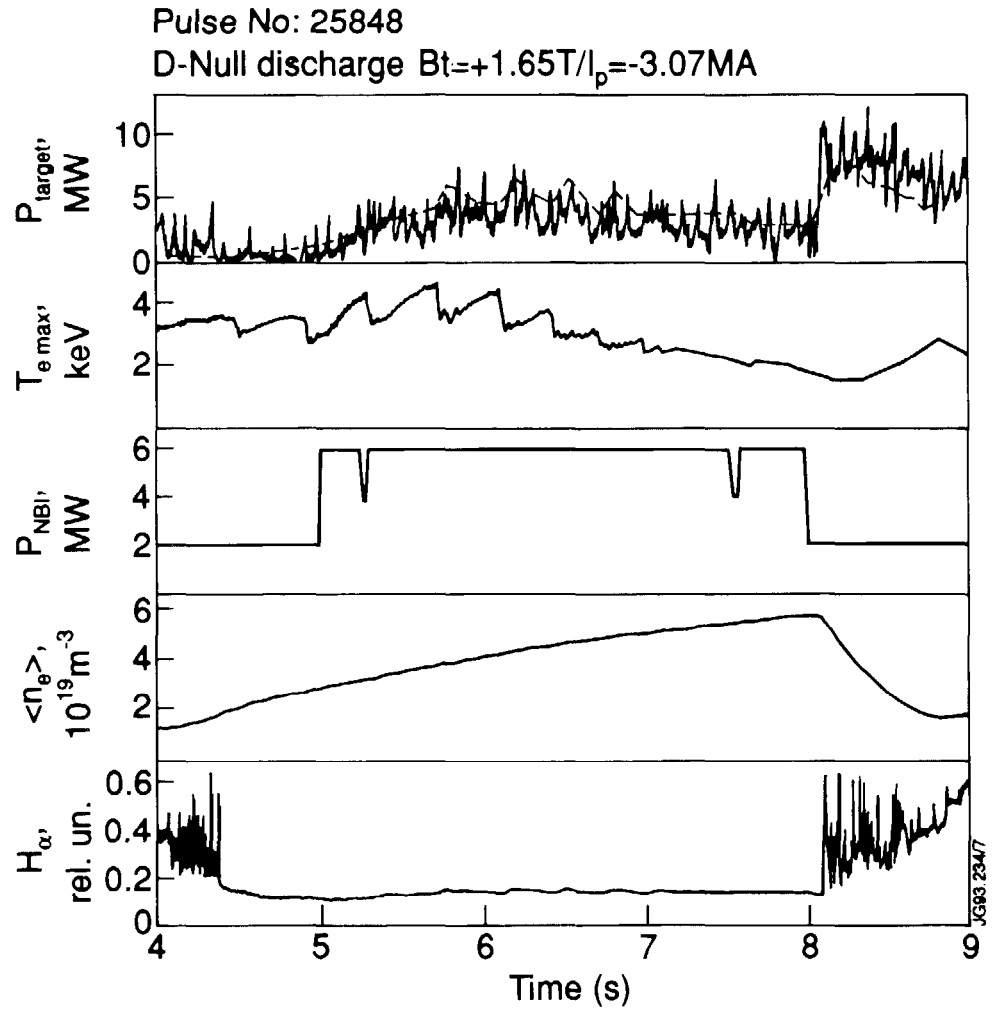

Fig. 8 Comparison between P_{exp} (solid line on the top plot) and $P_{in}-P_{rad}-\dot{W}$ (dashed-dotted line). Other parameters shown are: maximum electron temperature, $T_{e\,max}$, input NB power, volume averaged density, $<n_e>$, and H_α spectral line intensity from a vertical line looking at the divertor.